3-AXIS ACCELERATION SWITCH FOR TRAUMATIC BRAIN INJURY EARLY WARNING

L. J. Currano[1], C. R. Becker[1], G. L. Smith[1], B. Isaacson[2], and C. J. Morris[1]
[1]U.S. Army Research Laboratory – U.S.A.
[2]General Technical Services (for ARL) – U.S.A

ABSTRACT

This paper reports on the design, fabrication, and testing of a 3-axis acceleration switch intended to serve as an early warning for traumatic brain injury (TBI). Mild TBI (colloquially termed "concussion") resulting from rapid acceleration of the skull has been rising in the public consciousness with recently increasing awareness of the dangers and long-term health risks associated with it. The sensor described here is an array of acceleration switches designed to cover the range of acceleration associated with TBI, and to do so with no external power draw until an acceleration event within this range occurs.

INTRODUCTION

The U.S. Center for Disease Control and Prevention estimates that 1.7 million people sustain a traumatic brain injury annually in the United States alone, from auto accidents, slip-and-falls, contact sports, and other sources [1]. There are not always gross physical symptoms of TBI, so an early warning sensor is valuable to encourage victims to receive medical attention, especially in high-risk situations like American football or ice hockey.

Miniature accelerometers are widely available, but require a constant power draw. The 3-axis acceleration switch is useful for TBI monitoring because it requires very little power. In contrast to the wide variety of high-resolution MEMS accelerometers available, acceleration switches draw current only when an acceleration event occurs. Therefore the size of the battery (and the overall system) can be very small. This is important because the sensor should be in intimate contact with the head for optimal coupling and simpler data evaluation. Research by Ted Knox and colleagues at AFRL has shown that inside the ear canal is a promising sensor location [2], but the sensor and associated electronics must be very compact (<5mm) to fit.

The lower power consumption and subsequently smaller battery required make acceleration switches attractive for this application, so the sensor/data recorder/battery system can fit into an earplug. Figure 1 shows a comparison of expected battery lifetime with a 35mAh coin cell battery, showing ~100x better lifetime with an acceleration switch (inherent assumptions in this analysis: Freescale MCF51QE128 microcontroller in low-power state except during an event; analog accelerometer requires constant A/D power; each recorded event requires full-power wakeup of electronics for 2 seconds). The tradeoff for the longer battery lifetime, of course, is resolution since an acceleration switch by nature only tells whether an acceleration event has exceeded a defined threshold. For early-warning or trigger/wakeup-type applications, however, low resolution is an acceptable tradeoff for small form factor.
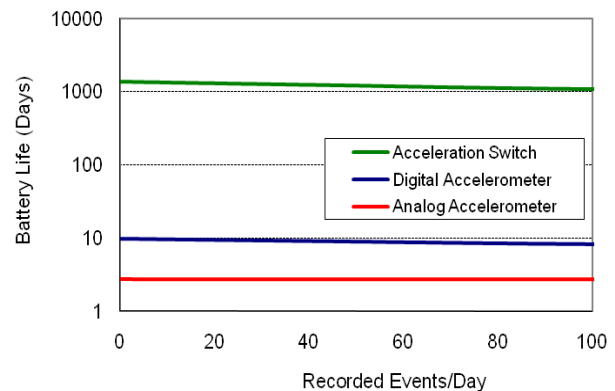

Figure 1: Estimated battery lifetime comparison for acceleration recording systems using analog accelerometer (freescale MMA7331LC), digital accelerometer (ADIS16204), and acceleration switch array. Accelerometers chosen as representative of low-power commercially-available sensors.

Acceleration switches were one of the earliest MEMS devices [3]. There has been periodic research on MEMS acceleration switches of various types throughout the last 30 years, but every type/configuration has been a single axis sensor (e.g., [4-7] among several others).

For TBI monitoring, the acceleration sensor should be a three-axis device as the impact can arrive from any direction. In order to keep the system size as small as possible, we used a spiral spring/annular mass system based on an impact switch originally designed by one of the authors (Mr. Smith) for fuzing applications [8]. The size of the mass and shape of the spring have been reduced and the fabrication process re-engineered for this work to better fit the very limited form factor required by the intended in-ear application.

In the current design, the annular mass has contacts arranged on each side (+x/-x/+y/-y) and above and below the mass (+z/-z) as shown in Fig. 2. The device is actually made up of six separate electrical switches with a common pole (one each between the anchor of the mass and each of the individual, isolated contacts). Thus the direction of the acceleration can be determined by which contact the switch touches.

The shape of the spiral springs that suspend the mass has been designed through finite element modeling to fit a particular acceleration threshold level. On each 3mm x 3mm die, 5 devices are included, designed to close at 50g/100g/150g/200g/250g thresholds. Thus the magnitude of the acceleration can be determined to be within the bounds of the thresholds of the highest switch that closes and the lowest switch that does not close (e.g., between 100g and 150g if the 100g device closes but the 150g device does not).
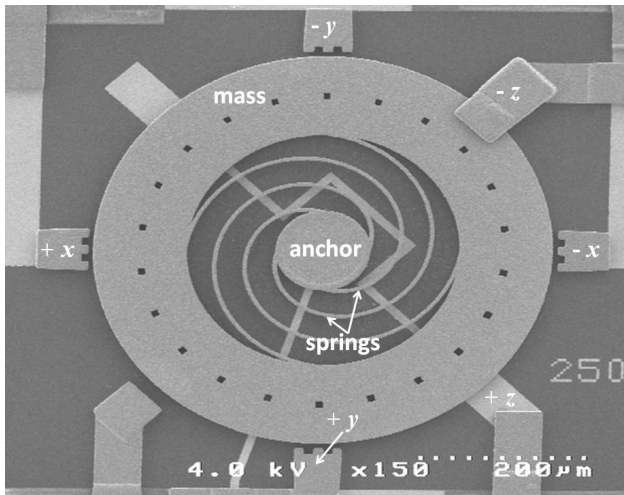
Figure 2: Acceleration switch with x, y, and z, contacts for 3-axis operation.

FABRICATION

The mass, springs, and contacts of the device are all surface micromachined from electroplated gold. The fabrication process proceeds as follows (Fig. 3): to begin, an insulating SiO_2 layer is deposited on a silicon substrate to effectively isolate each of the contacts from the mass and from each other. Then a Ti/Pt layer is deposited and patterned via liftoff to form the electrical interconnects, bondpads, anchors, and the z-axis contact positioned below the mass (Fig. 3a). A 10nm Cr/50nm Au seed layer is sputtered onto the wafer, then the Au contacts are patterned photolithographically and electroplated to approximately 5µm (Fig. 3b). The photoresist layer is stripped away and the gold seed layer is removed with diluted gold etchant, then the chromium adhesion layer is removed with diluted chromium etchant.
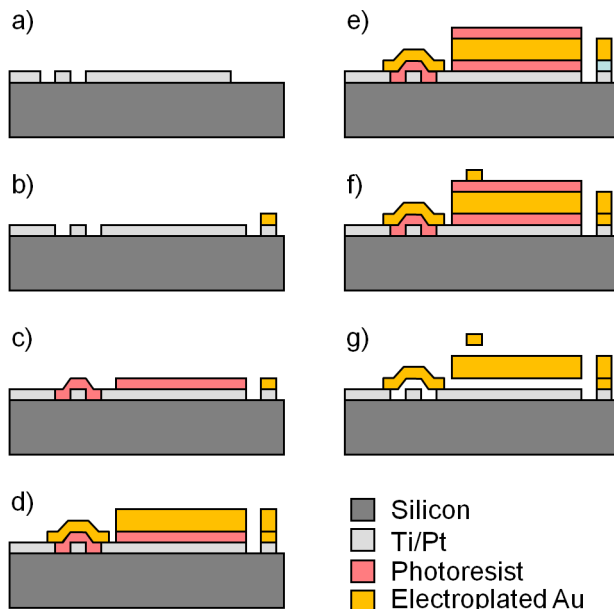

Figure 3: Fabrication process flow for acceleration switch.

Next a 6 µm thick sacrificial photoresist layer is deposited and patterned in the region of the mass and springs (Fig. 3c). We use a two-layer deposition of AZ5214 photoresist, with a UV-stabilization step after each of the layers. The UV-stabilization makes the photoresist impermeable to developers and acetone so it stands up to future photolithographic processing, but can still be removed with an oxygen plasma etch at the end of the process [9]. We use two layers because the UV-stabilization process causes bubbling of thick resist layers as the solvents leach out from deep inside the film. Two thinner layers on top of each other eliminates this problem as long as the first one is UV-stabilized before depositing the second. The sacrificial photoresist includes a circular opening at the center for the spring anchor.

Next another Cr/Au seed layer of the same thickness as the first plating step is sputtered onto the wafer. The mass, springs, and anchor are patterned in AZ9245 resist approximately 10µm thick, then electroplated in a gold plating bath to a thickness of 8µm (Fig. 3d). After stripping the plating mold resist using acetone (which does not remove the UV-stabilized sacrificial resist), the gold/chromium seed layer is once again removed using diluted wet etchants. A second sacrificial layer is deposited over the edge and on top of the mass, as a spacer for the z-axis contact that will be positioned above the mass (Fig. 3e). One more seed layer is deposited and a final electroplating mold patterned for the top contact. The top contact is plated to a thickness of approximately 4µm, then the photoresist is removed with acetone and the seed layer removed with diluted wet etchants (Fig. 3f). Finally the device is released via a series of 20 minute oxygen plasma ashes with cooling periods in between to keep the sacrificial resist from burning before it can be removed (Fig. 3g).

RESULTS
Fabrication

One important aspect of the fabrication process that proved critical in making these devices was the use of projection lithography rather than contact lithography. In projection lithography the focal plane for the mask image can be shifted up or down depending on the location of the substrate, whereas with contact lithography the effective focal plane is always the mask plane itself, and the image on the wafer is always defocused slightly due to diffraction. The defocus becomes worse as the distance from the mask to the actual desired image plane increases due to topography, thicker photoresist, etc. Accurately resolving the 4µm features in a 10µm thick photoresist film proved impossible with our contact lithography setup, but with some tweaking to the mask dimensions and exposure parameters, a 5x I-line stepper was able to produce a 4.7µm spring feature.

The type of electroplating solution used was also an important to the accurate reproduction of the design. We initially used Technic TG-25, a sulfite-based gold plating solution. However, the alkalinity of the TG-25 solution actually was found to attack the AZ9245 photoresist and effectively widen the features as the plating thickness/time increased. The result was a mushroom-like profile that makes fine feature resolution impossible, as shown in Fig. 4. We switched to TG-25E solution, which has a neutral pH, and achieved much better feature reproduction as
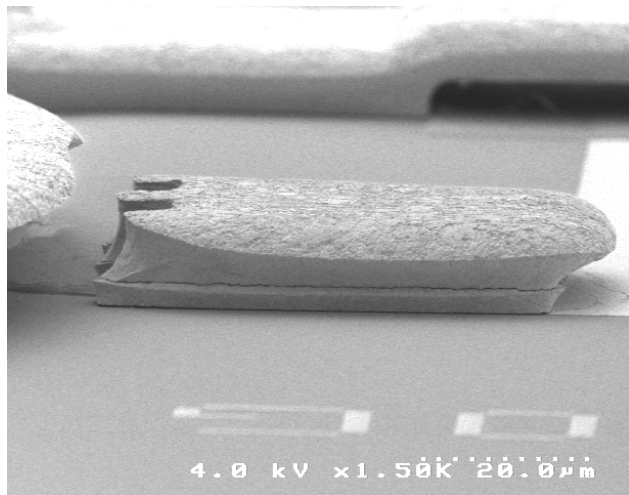
485

shown in Fig. 5.

Figure 4: Plated contact using TG-25, which attacks resist and widens features towards the top.
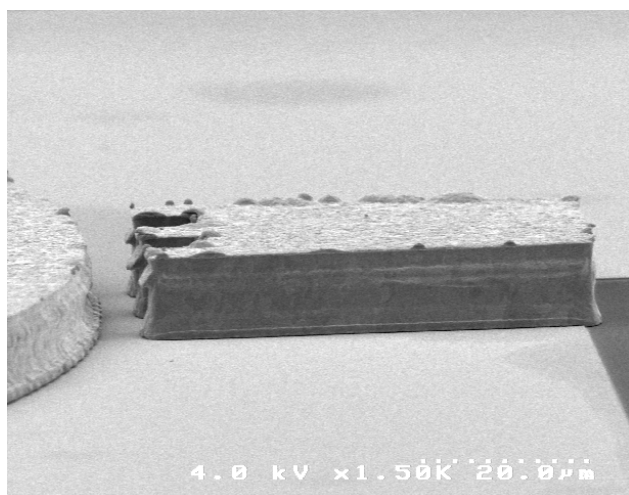

Figure 5. Plated contact using TG-25E gold plating solution, which is neutral and does not degrade photoresist.

The gold etchant used also was critical to the successful fabrication of these devices. The gap between the mass and the anchor is only 100μm wide, and the gaps between the individual springs is much smaller than that in some places. Incomplete wetting of the surface in between the springs in initial attempts with Transene GE-8148 left the gold seed layer unetched in some places. Transes manufactures a version of GE-8148 with an added surfactant, which eliminated all of the wetting problems and adequately removed all of the seed layer gold from between the springs.

Testing and Performance

The acceleration switches were tested on a GHI Systems Linear Shock Machine 100 benchtop acceleration table. A reference accelerometer screwed into a threaded hole on the table provided high resolution truth data to confirm the actual trigger thresholds. The acceleration switch wafer was cleaved into individual die, and the die were each packaged in dual-inline packages (DIP). These

were inserted into a socket on a printed circuit board, which was in turn bolted to the acceleration table. A voltage divider was constructed with a 2.15kΩ resistor in series with the acceleration switch. A DC voltage was applied across the voltage divider, and the voltage across the 2.15kΩ resistor was monitored using the same data acquisition system as the accelerometer to ensure accurate time synchronization. Thus the switch closure is detected as a step increase in voltage, and the switch re-opening is detected as a step decrease in voltage back to zero volts. A representative output from one test of the 50g nominal design threshold device is shown in Fig. 6 along with the reference accelerometer data which shows the actual applied acceleration time-history.
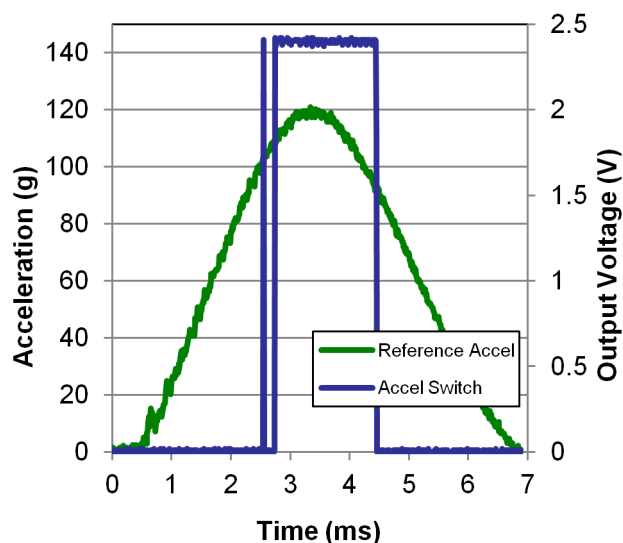

Figure 6: Representative output from acceleration switch (50g nominal design threshold) as monitored through voltage divider.

Notice from Fig. 6 that the center of the switch-closure curve is shifted right with respect to the time axis. This represents the finite mechanical delay in the response of the acceleration switch. There is a delay in both closing and opening as the mechanical system cannot respond infinitely fast. The center of the switch closure data is 255μs later than the center of the accelerometer data, reflecting the lower resonant frequency of the acceleration switch. We cannot achieve acceleration pulse widths this short with our acceleration table and therefore have not directly evaluated the minimum pulse width, but it is expected to be on the order of the switch closure delay.

To obtain an accurate measure of the actual switch closure threshold, the acceleration applied by the shock table was first set to a level below the threshold, then gradually increased in increments of 2-5g until the switch was observed to close. The measured threshold is defined as the lowest applied acceleration that causes the switch to close and a voltage to be observed across the 2.15kΩ resistor in the voltage divider. The x-axis positive and negative thresholds for one full die are shown in Fig. 7, with the values on the x-axis corresponding to the nominal (design) values. Within this one die, the positive and negative thresholds match fairly well, with the maximum deviation of about 10%. The y-axis thresholds are

generally close to the *x*-axis thresholds as well, as expected since the design uses 4 springs arranged at 90 degree axisymmetric intervals around the anchor. The actual match of the measured threshold to the designed threshold is not exact, with the nominal 50g device actually closing at 97.5g. This is the largest gap between the designed and measured threshold for the devices on this die, but there is some deviation in all but the 200g design. Adjustments will be made in future designs to better achieve the target acceleration thresholds.
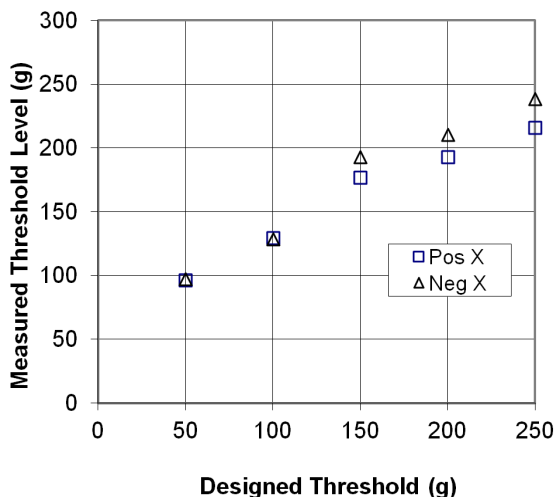

Figure 7. X-axis measured vs. designed thresholds for one die.

The z-axis is another matter entirely, given that the spring is bending in a completely different way out-of-plane than in-plane and the gaps between the mass and the contacts are defined in a completely different way as well. An attempt was made to match the in-plane and out-of-plane stiffnesses and gaps, but the springs widened during the lithography process to approximately 6μm. This reduced the ratio of the out-of-plane stiffness to in-plane stiffness, and the *z*-axis thresholds were much lower than the *x*- and *y*-axis thresholds as a result (~10-40g as opposed to ~90-230g for the in-plane axes). A redesign is currently underway to address this mismatch.

CONCLUSION

We have presented a new 3-axis acceleration switch design well-suited for traumatic brain injury detection due to its low-power and small form factor nature. A 3mm x 3mm die with 5 acceleration thresholds was fabricated and tested, with the measured acceleration thresholds in the *x*- and *y*-axes agreeing well with each other. The *z*-axis thresholds are significantly lower than the *x*- and *y*-axis better match the realized spring dimensions to the actual spring dimensions. The switch closure delay is estimated at 255μs for the 50g design, and should be lower for the other designs given the inverse relationship of natural frequency to acceleration sensitivity. thresholds in the current devices. A redesign is underway to correct for this by adjusting the fabrication process to better control the spring dimensions during photolithography.

Submitting author: L.J. Currano, U.S. Army Research Laboratory, Mailstop RDRL-SER-L, 2800 Powder Mill RD, Adelphi, MD 20783 USA; Tel: +1-301-394-0566; Fax: +1-301-394-1559; E-mail: luke.j.currano.civ@mail.mil.

REFERENCES

[1] M. Faul, L. Xu, M.M. Wald, and V.G. Coronado, *Traumatic Brain Injury in the United States: Emergency Department Visits, Hospitalizations, and Deaths 2002-2006,* Atlanta (GA): Centers for Disease Control and Prevention, 2010.
[2] T. Knox, "Validation of earplug accelerometers as a means of measuring head motion," in *Proc. of Motorsports Engineering Conference and Exposition*, Dearborn, MI, Nov. 30- Dec. 2, 2004, paper 2004-01-3538.
[3] W. Frobenius, S. Zeitman, M. White, D. O'Sullivan, and R. Hamel, "Microminiature ganged threshold accelerometers compatible with integrated circuit technology," *IEEE Transactions on Electron Devices* vol. 19, pp. 37-40, 1972.
[4] Y. Loke, G.H. McKinnon, and M.J. Brett, "Fabrication and characterization of silicon micromachined threshold accelerometers," *Sensors and Actuators A* vol. 29, pp. 235-240, 1991.
[5] J. Noetzel, T. Tonnesen, T.W. Benecke, J. Binder, and G. Mader, "Quasianalog accelerometer using microswitch array, *Sensors and Actuators A* vol. 54, pp. 574-578, 1996.
[6] S. McNamara and Y.B. Gianchandani, "LIGA-fabricated 19-element threshold accelerometer array," *Sensors and Actuators A* vol. 112, pp.175-183, 2004.
[7] L. J. Currano, M. Yu, and B. Balachandran, " Latching in a MEMS shock sensor: modeling and experiments," *Sensors and Actuators A*, vol. 159, pp. 41-5, 2010.
[8] G.L. Smith, "Micromechanical Shock Sensor," U.S. Patent Application 12/964,131, 2011.
[9] T. P. Takacs, J. Pulskamp, and R. Polcawich, "UV Baked/Cured photoresist used as a sacrificial layer in MEMS fabrication," Army Research Lab Technical Report ARL-MR-60, 2005.